2'-deoxyuridine-5'-monophosphate substrate displacement in thymidylate synthase through 6-hydroxy-2*H*-naphtho[1,8-bc]furan-2-one derivatives

Stefania Ferrari[1], Samuele Calò[1], Rosalida Leone[2†], Rosaria Luciani[1], Luca Costantino[1], Susan Sammak[1], Flavio Di Pisa[2], Cecilia Pozzi[2], Stefano Mangani[2], M. Paola Costi[1]*

[1] Department of Life Science, University of Modena and Reggio Emilia, Via Campi 183, 41125 Modena, Italy. [2] Department of Chemistry, University of Siena, Via Aldo Moro 2, 53100 Siena, Italy.

SUPPORTING INFORMATION

Content:

Scaffold identification: database search, scaffold selection.

In this work we aimed to find new possible scaffolds starting from 1,8-naphthalic anhydride (**1**). Scifinder was searched using the substructure search method (Figure S1). The retrieved results (>1000) were filtered based on: (I) chemical stability of the structure; (II) suitability for further derivatization (scaffold-like structure, presence of reactive functional groups, absence of functional groups that can compete in the same reaction, possible chemical modification reported in literature); (III) commercial or synthetically availability; (IV) not already being explored in our laboratory.

A number of possible scaffolds emerged, and compound **2** was chosen for further synthetic elaboration (Scheme 2).

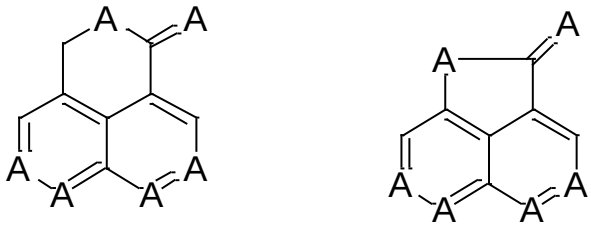

Figure S1. Queries used in Scifinder searches; A = any atom.

Library design

An ensemble of acyl chlorides were selected for esterification of hydroxyl group on position 6. The Acx2002Prod database (ChemOffice Ultra 7.0, Cambridge Soft corporation, htpp://www.cambridgesoft.com) was searched for all the commercial available aliphatic, cicloaliphatic, aromatic and heteroaromatic acyl chlorides. The available compounds, 737 acyl chlorides, were first filtered in order to avoid to have (i) more functional groups that can compete in the same reaction; (ii) chiral carbon atoms; (iii) groups near the reactive center that may cause steric hindrance; (iv) metal or organometallic groups; (v) too big or complex structures. The remaining 195 acyl chlorides were grouped on the base of their calculated molecular properties (MW, LogP, solubility) (ACD/Lab 6.0, Advance Chemistry Development Inc) and structural features. Finally the set of fragments (Table 1) were selected base on their molecular diversity, variability in their calculated molecular properties and their real commercial availability (no too costly or rare compounds).

X-ray crystallographic studies.

EcTS–dUMP-3 ternary complex. The EcTS-dUMP-**3** complex maintains the same structure of the native enzyme (PDB ID: 3TMS; PDB ID: 1F4B) showing a root mean square deviation of the backbone atoms within 0.37 Å from the two structures. [S1-S2]

The 264 amino acids of the polypeptide chain are all visible in the electron density maps, although in some of the loops, like the hairpin loop Glu14-Gly23, the electron density is weaker and some side chains of exposed Arg, Lys and Glu residues are not visible in the electron density map. A Fourier difference map (ΔF map) phased with the protein model alone shows significant electron density (3-5 times above σ) inside the active site cavity. The density appears flat in shape and quite extended, consistent with the presence of one molecule of **3** bound to the cavity. However, the density does not have the details expected at the nominal resolution of the structure and suggests that the inhibitor is bound in non-specific mode with different orientations in the active site cavity. The ΔF map reported in Figure 1 defines quite well the location of the naphtho[1,8-*bc*]furan-2-one moiety of **3** whereas there is little electron density for the para-nitro-benzoyl group suggesting that the molecule presents rotational disorder around the naphtho-furanosyl plane. A positive maximum of electron density appears in a position compatible with a nitro group on the aromatic ring and this feature has been used to model the whole molecule in the conformation reported in Figure 1. The molecule of compound **3** has been refined with 50% occupancy that gives atomic displacement parameters (ADPs) similar to those of the surrounding atoms.

The ΔF map indicates that the naphtho-furanosyl ring of **3** is located close to Cys146 sulfur (at about 3.3Å), in a hydrophobic environment defined by Trp80, Trp83, Leu143, Ile79 and Tyr94. The same electron density map does not shows any feature attributable to a dUMP molecule bound in the active site. On the contrary, positive electron density is clearly visible elongating from the usual phosphate binding site of dUMP located between Arg21-Arg166 of one subunit and Arg126'-Arg127' of the symmetry related subunit in the dimer and extending with the nucleoside moiety outside the active side cavity towards the solvent and H-bonded to Asp122', as shown by Figure S2. Although the electron density is not complete for the whole ribose and purine moieties (few atoms missing) of dUMP, it is sufficient to build a model that refines to reasonable values of ADPs with occupancies varying from 30% to 60%.

The present crystal structure indicates that the ribose and purine moieties of dUMP are displaced from the active site cavity and exposed to solvent, while the phosphate group is bound to the usual site between the side chains of Arg166 and Arg126’ of the partner subunit. It is possible that the phosphate side is partially occupied also by sulfate from the crystallization solution. A similar

binding mode of dUMP was already observed by Lebioda and collaborators for the analog FdUMP molecule co-crystallized with the Val3Phe mutant of hTS (PDB ID: 3EJL) [S3]. In that instance they showed that the mutation Val3Phe strongly compromises dUMP binding capability to hTS. Our result indicates that also bulky inhibitors like **3**, able to occupy a large portion of the active site close to Cys146, do not allow the binding of dUMP within it. (Figure S3)

Implication for further drug design. Compound **3** forms eight H-bonds with the side chains of six protein residues (Glu58, Tyr94, His147, Gln165, Asp169 and Asn177) and two H-bonds with the carbonyl oxygen of Ser167 and Asp169 crystallized in the active site through the nitro moiety and the furanone ring of the tricycle moiety. Moreover it interacts withPhe62, Ile79, Trp80, Trp83, Leu143, Cys 146, Cys168, Gly173 and Leu174. (Figure S2).

The structure of the ternary complex EcTS-dUMP-**3** enables to define the binding site for this family of inhibitors and to identify a new binding mode for the dUMP substrate.

This inhibitor accommodates the large naphto-furanosyl aromatic moiety in a lipophylic pocket defined by Trp80, Trp83, Leu143, Ile79 and Tyr94. This binding mode occludes the most part of the EcTS cavity preventing the access to the catalytic Cys146 and at the same time hindering the binding of dUMP within the active site. On the other hand, the benzoyl moiety of this molecule appears to be devoid of chemical determinants able to make specific interactions within the EcTS cavity. In the structure, this part of the inhibitor is poorly defined and multiple binding modes appear to be possible.

The newly found binding site for the dUMP substrate is located at the interface of the two symmetry-related subunits in a solvent exposed site. The dUMP phosphate group is linked in the usual site formed by Arg21, Arg166 of one subunit and Arg126', Arg127' of the facing subunit but with the nucleoside moiety directed out of the active site cavity towards the second subunit. However, this part of the molecule is not well defined and suggests the occurrence of multiple conformations.

The crystal structure of the described complex, highlights the usefulness of the naphto-furanosyl moiety as a scaffold to design more potent TS inhibitors and suggest to use the polar groups present in the active site cavity like Glu58, Tyr94, His147, Asn177 to achieve higher binding affinity. The observed binding of the dUMP molecule also suggests that “surface” inhibitors of EcTS might be designed starting from the phosphate binding site and exploiting the contacts shown by the dUMP molecule, at the surface of the EcTS dimer, with residues like Asp122', Asp124' and Ser125'.

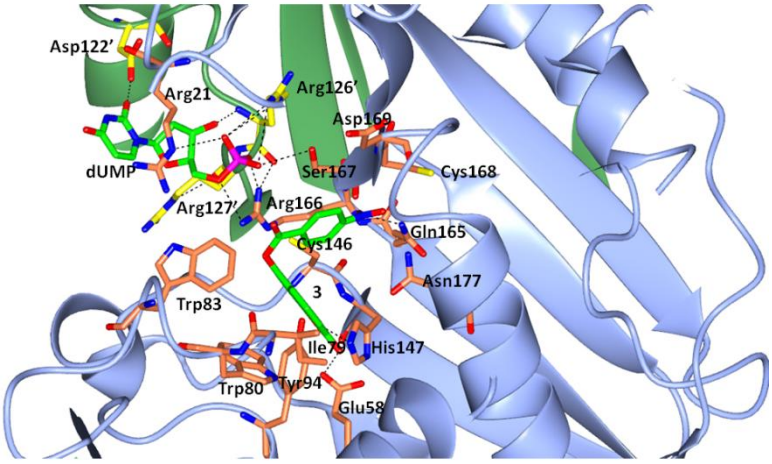

Figure S2. View of the EcTS-dUMP-**3** ternary complex (PDB-ID: 4LRR) active site with **3** and dUMP bound. The region of the active site where **3** (green carbons) is bound is represented by the side chains the interacting residues (coral carbons). The dUMP binding site consists of Arg21 and Arg166 from one subunit (coral carbons) and Asp122', Arg126' and Arg127' from the symmetry-related subunit (yellow carbons). H-bonds involving **3** and dUMP are represented as black dashed lines. Water molecules have been omitted for clarity. The two symmetry-related EcTS molecules are represented as pale blue and green ribbons, respectively.

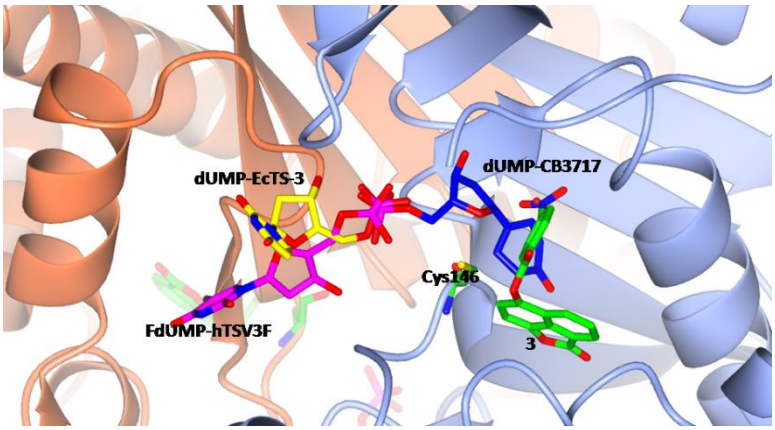

Figure S3. Comparison of classical and alternative dUMP (and FdUMP) binding modes. dUMP (C atoms in blue) in ternary complex with EcTS and a folate-analog inhibitor CB3717 (PDB ID: 2TSC); dUMP (C atoms in yellow) in ternary complex with EcTS and compound **3** (PDB-ID: 4LRR); FdUMP (C atoms in magenta) in binary complex with hTS Val3Phe mutant (PDB ID: 3EJL). The symmetry-related EcTS subunits are shown as ice-blue and coral ribbons. C atoms of compound **3** are shown in green.

Table S1. Data collection and refinement statistics.

Data collection statistics (values in parentheses refer to the highest resolution shell)	
Compound, PDB code	EcTS-dUMP-**3,** 4LRR
Beamline, wavelength (Å)	ESRF ID 14-1 0.934
Space group, Z	cubic $I2_13$, 12
Cell dimensions (Å)	a=131.18
Resolution range (Å)	65.65 - 2.41 (2.57 – 2.41)
Total reflections	156238 (23101)
Unique reflections	14375 (2307)
Completeness(%)	100 (100)
R_{merge} *, %*	6.5 (17.5)
Multiplicity	10.9 (10.0)
I/σ(I)	6.9 (2.8)
Refinement statistics (values in parentheses refer to the highest resolution shell)	
Resolution range (Å)	37.87 – 2.41 (2.47 -2.41)
Reflections number	13989 (1041)
R cryst (%)	16.4 (16.6)
R free (%)	22.1 (25.2)
Protein atoms	2141
Ligand atoms: F9, dUMP	24, 20
Sulfate ions	8
Water molecules	169
Mean B factor ($Å^2$)	25.91
Rmsd bond lengths (Å)	0.018
Rmsd bond angles (°)	2.087
Rmsd planes (Å)	0.009
Rmsd chiral volumes ($Å^3$)	0.121
Ramachandran plot %	
Most favoured	97.3

Allowed	2.7
Disallowed	0.0

Experimental Section

TS activity inhibition profile evaluation. Proteins were purified as described previously. [S4-S10] MTHF was a gift from Merck & Co (Switzerland); all other reagents were purchased from different companies at the highest purity grade possible. Kinetic experiments were conducted under standard conditions. [S11] Inhibition experiments were conducted by measuring the effects of different inhibitor concentrations on the initial rate of the enzymatic reaction, in the presence of a limited concentration of the MTHF or dUMP substrates. Reactions were initiated by addition of the enzyme. K_i values were detected, showing competitive inhibition with respect to MTHF and dUMP substrates. [S12-S13]. K_i values are expressed as mean ± S.E.M. of 3 determinations. Stock solutions of each inhibitor were freshly prepared in DMSO. The DMSO concentration was kept below the concentration known to affect enzymatic activity (5% for TS).

Crystallization conditions. Diffraction-quality crystals of EcTS (MW 30523 Da, due to N-terminus carboxylation) complexes have been obtained from a sitting-drop setup. The protein solution contained 7 mg/mL of enzyme, 40 mM dUMP and 2 mM inhibitor (compund **3**) solubilized in a 10:1 v/v mixture of water/ DMSO. The total amount of DMSO present in the crystallization solution has been optimized in order to maximise inhibitor solubility and to avoid protein denaturation. [S14-S15]

The reservoir solution contained 700 μL of a Bicine 0.1 M, (NH4)2SO4 3.2 M at pH 8.3. The drops have been prepared by mixing 2 μL of EcTS/dUMP/inhibitor solution with 2 μL of the above reservoir solution. Small crystals were observed after four-five days and their growth was completed in about two weeks. For data collection the crystals were flash-frozen under a cold nitrogen stream at 100 K, by using as cryoprotectant the reservoir solution with added 20% ethylene glycol.

Data collection, processing and structure determination. Table S1 reports the data collection and refinement statistics of the analyzed dataset. The EcTs-dUMP-**3** data set has been collected using synchrotron radiation from the ESRF, Grenoble, France ID14-1 beamline with a wavelength of 0.934 Å and the ADSC Quantum 4 detector.

The data set was processed using MOSFLM 6.2 [S16-S17] and scaled with SCALA [S18].

The EcTS holoenzyme is dimeric and possess exact two-fold symmetry. The EcTS ternary complexes crystallize in the cubic $I2_13$ space group (space group n. 199) with the dimers sitting on the cell 12 special positions of point symmetry 2 so that he crystal asymmetric unit contains only

one EcTS subunit. The crystal structure was solved using the molecular replacement technique. The model used consisted of one EcTS subunit (PDB ID: 2TSC) where all the water molecules and ligands had been omitted. The correct orientation and translation of the molecule within the crystallographic asymmetric unit was determined with standard Patterson search techniques as implemented in the program MOLREP [S19]. The program readily provided an evident solution for the positioning for the molecule in the asymmetric unit. The refinement was carried out using REFMAC5 [S7, S20]. During the refinement cycles the model was subjected to manual rebuilding by using Coot [S21]

Water molecules have been added by using the standard procedures within the ARP/wARP suite. [S22] The stereochemical quality of the refined model was assessed using the program PROCHECK. [S23] The refinement statistics are reported in Table S1.

Figures were prepared with the program CCP4MG from the CCP4 suite. [S17]

Analytical data for compounds 5-13.

The purity of all materials was determined to be at least 95% by TLC, ^{1}H NMR and elemental analyses. The synthesis of compounds **5-13** was performed as for compunds **3** and **4** using Büchi Syncore® parallel synthesizer with yields in the range 30-45%. Elemental analyses were performed on a Perkin-Elmer 240C instrument and the results for C, H and N were within ± 0.4% of theoretical values. All synthesized compounds were characterized by ^{1}H NMR on Bruker DPX-200 MHz spectrometer operating at 200 MHz or Bruker Avance 400 at 400 MHz in solvents as noted. Chemical shifts are reported as δ values (ppm). *J* values are given in Hz. When peak multiplicities are given, the following abbreviations are used: s, singlet; d, doublet; t, triplet; q, quartet; m, multiplet; dd double doublet; br., broad peak.

(2-methylpropyl) (2-oxo-2*H*-naphtho[1,8-*bc*]furan-6-yl) carbonate (5). ^{1}H NMR (DMSO-d_6, 200 MHz) δ 8.48 (1H, d, *J* 8.0), 8.34 (1H, d, *J* 8.1), 8.03 (1H, t, *J* 8.0), 7.27 (1H, d, *J* 8.0), 7.03 (1H, d, *J* 7.9), 4.15 (2H, dd *J* 12.0, *J* 6.0), 1.60 (1H, m), 1.1 (6H, m). Anal. Calc. for $C_{16}H_{14}O_5$: C, 67.13, H, 4.93; found: C, 67.21, H, 4.96.

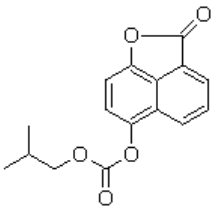

ethyl (2-oxo-2*H*-naphtho[1,8-*bc*]furan-6-yl) carbonate (6). ^{1}H NMR ($CDCl_3$, 200 MHz) δ 8.21 (1H, d, *J* 8.0), 8.19 (1H, d, *J* 8.0), 7.86 (1H, d, *J* 6.0), 7.42 (1H, d, *J* 8.0), 7.14 (1H, d, *J* 8.0), 4.37 (2H, q, *J* 7.0), 1.42 (3H, t, *J* 7.0). Anal. Calc. for $C_{14}H_{10}O_5$: C, 65.12, H, 3.90; found: C, 65.01, H, 3.94.

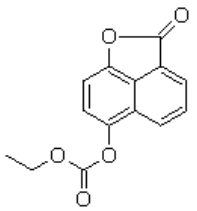

6-(2-propenoyloxy)-2-oxo-2*H*-naphtho[1,8-*bc*]furan (7). ^{1}H NMR ($CDCl_3$, 400 MHz) δ 8.22 (1H,

d, *J* 8.0), 8.10 (1H, d, *J* 8.0), 7.90 (1H, d, *J* 8.0), 7.40 (1H, d, *J* 7.0), 7.20 (1H, d, *J* 7.0), 6.80 (1H, dd, *J* 14.0, *J* 1.0), 6.50(1H, dd, *J* 14.0, *J* 7.0), 6.18 (1H, dd, *J* 8.0, *J* 2.0). Anal. Calc. for $C_{14}H_8O_4$: C, 70.00, H, 3.36; found: C, 70.18, H, 3.31.

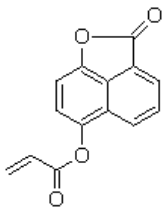

6-(2-furanoyloxy)-2-oxo-2*H*-naphtho[1,8-*bc*]furan (8). ^{1}H NMR ($CDCl_3$, 200 MHz) δ 8.20 (1H, d, *J* 8.0), 8.14 (1H, d, *J* 8.1), 7.83 (1H, dd, *J* 7.0, *J* 2.1), 7.72 (1H, dd, *J* 1.5, *J* 1.0), 7.46 (1H, d, *J* 7.3), 7.44 (1H, dd, *J* 3.5, *J* 1.5), 7.17 (1H, d, *J* 8.0), 6.64 (1H, dd, *J* 3.5, *J* 1.5). Anal. Calc. for $C_{16}H_8O_5$: C, 68.58, H, 2.88; found: C, 68.72, H, 2.93.

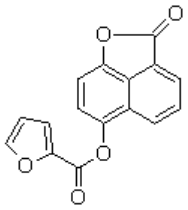

6-cyclohesanoyloxy-2-oxo-2*H*-naphtho[1,8-*bc*]furan (9). ^{1}H NMR ($CDCl_3$, 200 MHz) δ 8.18 (1H, d, *J* 8.0), 8.05 (1H, d, *J* 8.0), 7.83 (1H, d, *J* 8.0), 7.27 (1H, d, *J* 8.0), 7.12 (1H, d, *J* 8.0), 2.5 (1H, m) 2.20-1.00 (10H, m). Anal. Calc. for $C_{18}H_{16}O_4$: C, 72.96, H, 5.44; found: C, 72.85, H, 5.37.

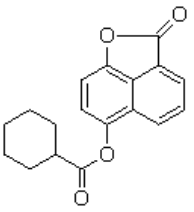

6-(3-trifluoromethyl-benzoyloxy)-2-oxo-2*H*-naphtho[1,8-*bc*]furan (10). ^{1}H NMR ($CDCl_3$, 200 MHz) δ 8.60 (1H, s), 8.52 (1H, d, *J* 8.0), 8.34 (1H, d, *J* 8.0), 7.94 (2H, d, *J* 8.0), 7.71 (1H, dd, *J* 7.0, 2.0), 7.43 (1H, d, *J* 8.0), 7.26 (1H, d, *J* 7.9), 7.01 (1H, d, *J* 7.9). Anal. Calc. for $C_{19}H_9F_3O_4$: C, 63.70, H, 2.53; found: C, 63.55, H, 2.58.

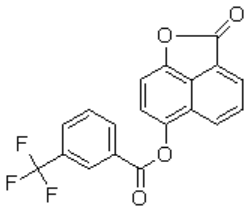

6-(1,3-benzodioxole-5-carbonyloxy)-2-oxo-2*H*-naphtho[1,8-*bc*]furan (11). ^{1}H NMR ($CDCl_3$, 200 MHz) δ 8.19 (1H, d, *J* 8.0), 8.10 (1H, d, *J* 8.0), 7.92 (1H, d, *J* 8.0), 7.87 (1H, d, *J* 8.0), 7.72 (1H, s), 7.41 (1H, d, *J* 8.0), 7.18 (1H, d, *J* 8.0), 6.94 (1H, d, *J* 8.0), 6.15 (2H, s). Anal. Calc, for $C_{19}H_{10}O_6$: C, 68.27, H, 3.02; found: C, 68.40, H, 3.01.

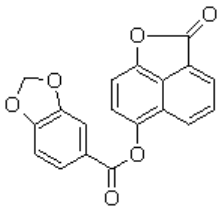

6-{4[(tryfluoromethyl)sulfanyl]benzoyloxy}-2-oxo-2*H*-naphtho[1,8-*bc*]furan (12). ^{1}H NMR ($CDCl_3$, 200 MHz) δ 8.36 (1H, d, *J* 8.0), 8.25 (2H, m), 8.09 (1H, d, *J* 8.0), 7.82 (1H, d, *J* 8.0), 7.79 (2H, m), 7.43 (1H, d, *J* 8.0), 7.18 (1H, d, *J* 8.0). Anal. Calc. for $C_{19}H_9F_3O_4S$: C, 58.46, H, 2.32; found: C, 58.30, H, 2.34.

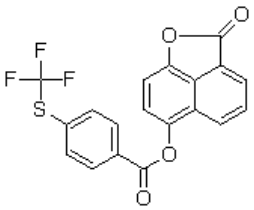

(2E) 6-(2-butenoyloxy)-2-oxo-2*H*-naphtho[1,8-*bc*]furan (13). ^{1}H NMR ($CDCl_3$, 200 MHz) δ 8.19 (1H, d, *J* 8.0), 8.08 (1H, d, *J* 7.9), 7.82 (1H, dd, *J* 7.9, *J* 2.1), 7.30 (1H, m), 7.16 (1H, d, *J* 7.8), 7.01 (1H, d, *J* 7.9), 6.20 (1H, d, *J* 14.0), 2.02 (3H, dd, *J* 7.0, *J* 2.0). Anal. Calc. for $C_{15}H_{10}O_4$: C, 70.86, H, 3.96; found: C, 70.69, H, 3.91.

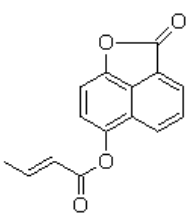

References

S1. Perry, K. M.; Fauman, E. B.; Finer-Moore, J. S.; Montfort, W. R.; Maley, G. F.; Maley, F.; Stroud, R. M. Plastic adaptation toward mutations in proteins: structural comparison of thymidylate synthases. *Proteins* **1990**, *8*, 315-333.

S2. Erlanson, D. A.; Braisted, A. C.; Raphael, D. R.; Randal, M.; Stroud, R. M.; Gordon, E. M.; Wells, J. A. Site-directed ligand discovery. *Proc. Natl. Acad. Sci. U. S. A.* **2000**, *97*, 9367-9372.

S3. Huang, X.; Gibson, L. M.; Bell, B. J.; Lovelace, L. L.; Peña, M. M.; Berger, F. G.; Berger, S. H.; Lebioda L. Replacement of Val3 in human thymidylate synthase affects its kinetic properties and intracellular stability. *Biochemistry* **2010**, *49*, 2475-2482.

S4. Ferrari, S.; Costi, M. P.; Wade, R. Inhibitor specificity via protein dynamics: insights from the design of antibacterial agents targeted against thymidylate synthase. *Chem. Biol.* **2003**, *10*, 1183-1193.

S5. Mangani, S.; Cancian, L.; Leone, R.; Pozzi, C.; Lazzari, S.; Luciani, R.; Ferrari, S.; Costi, M. P. Identification of the Binding Modes of N-Phenylphthalimides Inhibiting Bacterial Thymidylate Synthase through X-Ray Crystallography Screening. *J. Med. Chem.* **2011**, *54*, 5454–5467.

S6. Kealey, J. T.; Santi, D. V. Purification methods for recombinant Lactobacillus casei thymidylate synthase and mutants: a general, automated procedure. *Protein Expression Purif.* **1992**, *4*, 380–385.

S7. Maley, G. F.; Maley, F. Properties of a defined mutant of Escherichia coli thymidylate synthase. *J. Biol. Chem.* **1988**, *263*, 7620–7627.

S8. Pedersen-Lane, J.; Maley, G. F.; Chu, E.; Maley, F. High-level expression of human thymidylate synthase. *Protein Expression Purif.* **1997**, *10*, 256–262.

S9. Santi, D. V.; Edman, U.; Minkin, S.; Greene, P. J. Purification and characterization of recombinant Pneumocystis carinii thymidylate synthase. *Protein Expr. Purif.* **1991**, *2*, 350–354.

S10. Edman, U.; Edman, J. C.; Lundgren, B.; Santi, D. V. Isolation and expression of the Pneumocystis carinii thymidylate synthase gene. *Proc. Natl. Acad. Sci. USA* **1989**, *84*, 6503–6507.

S11. Pogolotti, A. L. Jr.; Danenberg, P. V.; Santi, D. V. Kinetics and mechanism of interaction of 10-propargyl-5,8-dideazafolate with thymidylate synthase. *J. Med. Chem.* **1986**, *29*, 478-482.

S12. Chou, T. Relationships between inhibition constants and fractional inhibition in enzyme-catalyzed reactions with different numbers of reactants, different reaction mechanisms, and different types and mechanisms of inhibition. *Mol. Pharmacol.* **1974**, *10*, 235-247.

S13. Segel, I. H. Enzyme Kinetics: Behaviour and Analysis of Rapid Equilibrium and Steady-State Enzyme Systems 1975, Wiley New York

S14. Jaspard, E. Role of protein-solvent interactions in refolding: effects of cosolvent additives on the renaturation of porcine pancreatic elastase at various pHs. Arch. *Biochem. Biophys.* **2000**, *375*, 220-228.

S15. Bhattacharjya, S.; Balaram, P. Effects of organic solvents on protein structures: observation of a structured helical core in hen egg-white lysozyme in aqueous dimethylsulfoxide. *Proteins* **1997**, *29*, 492-507.

S16. Leslie, A. G. W. Crystallographic. Computing V. (Moras, D., Podjarny, A. D. and Thierry, J.-C., eds) 1991, pp.50-61, Oxford University Press. Oxford.

S17. Collaborative Computational Project, No. 4, The CCP4 suite: programs for protein crystallography. Acta Crystallogr., Sect. D: Biol. Crystallogr. 1994, 50, 760–763.

S18. Evans, P. R. SCALA, continuous scaling program. *Joint CCP4 ESF-EACBM Newsl.* **1997**, *33*, 22–24.

S19. Vagin, A,; Teplyakov, A. MOLREP: an automated program for molecular replacement. *J. Appl. Crystallogr.* **1997**, *30*, 1022–1025.

S20. Murshudov, G. N.; Vagin, A. A.; Dodson, E. J. Refinement of macromolecular structures by the maximum-likelihood method. *Acta Crystallogr. Sect. D* **1997**, *53*, 240-255.

S21. Emsley, P.; Cowtan, K. Coot: model-building tools for molecular graphics. *Acta Crystallogr D Biol Crystallogr.* **2004**, *60*, 2126-2132.

S22. Perrakis, A.; Morris, R. J. H.; Lamzin, V. S. Automated protein model building combined with iterative structure refinement. *Nat. Struct. Biol.* **1999**, *6*, 458-463

S23. Laskowski RA, MacArthur MW, Moss DS, Thornton JM PROCHECK: a program to check the stereochemical quality of protein structures. *J Appl Crystallogr* **1993**, *26*, 283-291